PAPER

Check for updates

Preparation of biocompatible hydrogels reinforced by different nanosheets†

Taiga Ito,[a] Saki Endo,[a] Yoshiyuki Sugahara,[ab] Ryota Tamate [c]
and Régis Guégan [*d]

The impact of inorganic nanosheets with various chemical compositions and properties at different concentrations on the rheological properties and the gelation formation of a thermo-responsive hydrogel was investigated. F127 Pluronic triblock copolymers, with the structure $(EO)_{99}(PO)_{65}(EO)_{99}$ (EO: ethylene oxide and PO propylene oxide respectively), functionalized by dimethacrylate (F127-DMA) at a concentration of 25% was used in this study. After careful characterization by complementary techniques: transmission electron microscopy (TEM), atomic force microscopy (AFM), and X-ray diffraction of nanosheets derived from the peeling of layered materials (montmorillonite, organoclays and hexaniobate), the nanosheets were seen to be suitably dispersed in the hydrogels. The inclusion of hydrophobic nanosheets (*i.e.* those treated with the grafting of surfactants onto their surface: organoclays and hexaniobate) leads to a depression of the gelation temperature while the nanocomposites exhibit an enhancement of their elastic properties, as determined by rheological measurements. In contrast, the inclusion of hydrophilic nanosheet derived from raw montmorillonite engenders an opposite trend. The whole nanocomposites whose gelation temperature can be tuned by both the nature and concentration of the nanosheets were successfully photopolymerized allowing the formation of a 3D structure containing a large content of water. The results obtained in this study open new perspectives for possible uses of hydrogel-based nanocomposites as embedding matrixes for bio-organisms.

Introduction

Due to their biocompatibility, effective mass transfer and flexibility, hydrogels have received particular attention for possible uses in wearable devices and biosensors, and in tissue engineering, regenerative medicine, and drug delivery systems.[1–10] Among the hydrogels that can be applied in the medical field, physical gels (*i.e.* gels formed by physical bonds) showing a positive response feedback to thermal or electrical (change of ionic strength) stimuli are the most appropriate and interesting candidates. These hydrogels can be prepared through a 3D printing procedure allowing one to mimic the environment for living organisms, and to control complex conformations,[5,9–11] in which the injections, gelation time, temperature, viscosity, *etc.* represent important factors.[12,13]

aDepartment of Applied Chemistry, Waseda University, Tokyo, Japan

bKagami Memorial Institute for Materials Science and Technology, Waseda University, Tokyo, Japan

cCenter for Green Research on Energy and Environmental Materials, National Institute for Materials Science, Tsukuba, Japan

dGlobal Center for Science and Engineering, Waseda University, Tokyo, Japan. E-mail: regis.guegan@aoni.waseda.jp; regis.guegan@univ-orleans.fr

† Electronic supplementary information (ESI) available. See DOI: 10.1039/d1ra07604c

Thus, calcium alginate hydrogel was successfully used as an embedding matrix for bio-organisms. Nevertheless, the relatively fragile structure of the hydrogel is easily disrupted without a continuous supply of Ca^{2+}.[14,15] Reverse thermo-responsive hydrogels based on Pluronics® nonionic triblock copolymer of the structure $(EO)_x(PO)_y(EO)_x$, with x and y as the numbers of ethylene oxide (EO) and propylene oxide (PO) groups do not suffer from the requirement of a constant supply of ions and display the advantages of being both inexpensive and biocompatible. Among the different available Pluronics®, Pluronic F127 with a composition of $(EO)_{99}(PO)_{65}(EO)_{99}$ forms a gel by an increase of the volume fraction of the micelles or the temperature (affecting the water content in a sample and thus the concentration of F127). At a threshold volume fraction of 0.53, the packing in a cubic structure favours a close contact of the F127 micelles driving to the entanglements of the hydrophilic EO groups which in that way forms a gel. Other mechanisms were proposed for the gel formation implying the release of water bound to the PO groups with the increase of the temperature, leading to a gain of the entropy that induces the endothermic transition.[9,12,16,17]

However, the final properties of the hydrogels mainly depend on their mechanical properties that represent a central issue regarding their high-water content. One possibility consists of

the functionalization of the polymers with methacrylate groups for an improvement of the cross-linking or by the inclusion of inorganic particles that can form a cross-linked network as well as exemplary in the case of graphene oxide sheets in sodium alginate hydrogel nanocomposite.[18] Beyond a possibility to form an additional network, the inclusion of inorganic particles in hydrogels and more broadly polymers is recognized to improve the global mechanical properties (hardness of the materials with the presence of crystalline particles) as well as conferring additional features (optical, anisotropy…) depending on the nature and shape of the particles.[19–22]

Among the numerous types of inorganic nanosheets, nanosheets based on swelling clay minerals (montmorillonite for instance) show biocompatibility properties for being embedded in organic matrixes. As an exemplification of their biocompatibility, clay minerals are commonly used as excipient in drug formulations, drug delivery systems or protecting matrices for the preservation of pharmaceuticals.[19,21] The chemical modification of the clay mineral surface with the use of surfactant changes their hydrophilic behavior to hydrophobic or confers a dual hydrophilic–hydrophobic nature for cationic and nonionic surfactants respectively.[19,21,23] Hexaniobate double nanosheets with similar lateral size of about 1 micrometer as nanosheets derived from clay minerals, were already studied as reinforcers for hydrogels giving further anisotropic properties and other functional characteristics to the composite materials.[3,24] The hexaniobate surface coated with cationic surfactants displays a hydrophobic behavior while showing a certain biocompatibility as recent experiments of our group underscored. In addition, hexaniobate nanosheets show two layers organization, and thus are labelled as double nanosheets, that may strengthen the elastic properties of the resulting composite materials.

The inclusion of nanosheets in host matrices (hydrogels here) can be seen as host–guest materials where host–guest interactions represent a key point favoring the possible entanglements between colloids that can be multiplied or in contrast screened leading to the spread of the gelation on a wide range of temperatures with some domains that are impossible to reach using only bulk hydrogels.[25–29] Depending on the affinity and the strength of the interaction between host–guest materials as well as the proper dispersion of the nanosheets that can even form gels in solvents at high concentrations as recent studies pointed out,[26,29] the gelation can be shifted to low or high temperature while affecting the global elastic properties of the composites.

This study aims at investigating the impact of the inclusion of several nanosheets of different chemical natures (*i.e.* hydrophilic and hydrophobic) on the elastic properties as well as the gel formation of the Pluronic F127 triblock co-polymers, functionalized by dimethacrylate (F127-DMA). Thus, different nanosheets were prepared through the peeling of different layered materials: potassium hexaniobate and montmorillonite (MMT). In contrast to hydrophilic MMT nanosheets, hydrophobic organo-nanosheets are synthesized by the grating of surfactants: tetrabutylammonium (TBA) and pentaethylene glycol monodecyl ether ($C_{10}E_5$) onto hexaniobate and

montmorillonite for the obtention of TBA-hexaniobate and OMMT respectively. In addition to the understanding of the role of the nature of the nanosheets on the mechanisms of the gelation of F127 and its elastic properties, the photo-polymerization of the resulting composites is also discussed.

Materials and methods

Materials

Pluronic F-127 (Sigma-Aldrich), anhydrous toluene (Wako, 99.5%), trimethylamine (Wako, 99.0%), methacryloyl chloride (TCI, 90%), diethyl ether (Wako, 99.5%), montmorillonite (The Clay Science Society of Japan), pentaethylene glycol monodecyl ether ($C_{10}E_5$) (Sigma Aldrich, 97.0%), potassium carbonate (K_2CO_3) (Wako, 98.5%), niobium(v) oxide (Nb_2O_5) (Wako, 99.9%), hydrochloric acid (HCl) (Wako, 35.0%), tetrabutylammonium hydroxide solution (TBAOH) (Sigma-Aldrich, 40 wt%), and 2-hydroxymethyl propiophenone (TCI, 96.0%) were used in this study.

Synthesis of F-127-dimethacrylate (F-127-DMA)

The synthesis of F-127-DMA was performed in a similar way to that explained in the work of A. Saha *et al.*[9] Before the synthesis, 10.5 g of Pluronic F-127 was vacuum dried at 50 °C for 24 h. Then, 82.5 mL of anhydrous toluene was added to F-127 under a N_2 atmosphere. Furthermore, 2.04 mL of triethylamine was added to the solution, and it was cooled it down to 0 °C. Next, a mixed solution 7.5 mL of anhydrous toluene and 1.44 mL methacryloyl chloride was added dropwise over 30 minutes through a funnel under stirring. After completion of the dropping, the mixture was stirred at 0 °C for 1 h, and then continuously stirred at room temperature (rt) for 24 h or more under a N_2 atmosphere. Then, a vacuum-filtration was performed at 40 °C. The collected filtrate was concentrated under reduced pressure, another 90 mL of toluene was added, and the mixture was warmed up to 40 °C. After repeating the previous steps related to filtration and decompression three times, the filtrate was concentrated under reduced pressure (50 hPa) and 30 mL of toluene was added. A precipitate was formed from the solution with an excess of 210 mL of diethyl ether. Centrifugation was performed twice at 4400 rpm for 15 min, and the obtained white precipitate was dried under ambient conditions for 12 h. Finally, it was dried under reduced pressure at 40 °C for 24 h, and the F-127-DMA product was obtained.

Preparation of dispersion of organoclay nanosheets

Montmorillonite (Kunipia-F) was dispersed (4 g) in 100 mL of water.[16] And 1.06 mL of $C_{10}E_5$ nonionic surfactant was added to the solution and stirred overnight. The obtained dispersion was centrifuged twice at 5500 rpm and dried at 80 °C for 48 h. Water was added to rinse the solid organoclay (OMMT), which was dispersed again in water to prepare the dispersions of organo-montmorillonite (OMMT) nanosheets at concentrations of 1, 2, 5, 10 g L^{-1}. In addition, hydrophilic montmorillonite (MMT) was dispersed in water at the same concentration as OMMT to obtain the hydrophilic nanosheet dispersions.

Preparation of dispersion of hexaniobate nanosheets

First, 1.48 g of K_2CO_3 and 4.04 g of Nb_2O_5 were mixed with water in a mortar for 1 h. Then, the sample was air-dried and burned in a crucible at 1100 °C for 10 h. The resulting collected white powder was washed with water and centrifuged 5 times at 3000 rpm for 5 min. The white sample was dried and layered hexaniobate (KNbO) was obtained. KNbO was stirred in 2.5 M HCl for 3 days, to substitute the K^+ ions with hydronium ions within the niobate layers. A TBAOH solution (40 wt%) was added to the layered niobate materials and the dispersion was stirred until the pH reached 10.[17,18] The supernatant of the dispersion after dialysis for 3 days was freeze-dried to a powder state, and water was added to prepare a dispersion of NbO nanosheets at concentrations of 1, 2, 5, 10 g L^{-1}.

Mixing of hydrogel and nanosheets

Untreated F-127 or F-127 DMA and water were mixed at 4 °C to prepare hydrogels at different concentrations (10–40 wt%). In addition, F-127-DMA was mixed with some dispersions of OMMT nanosheets, unmodified montmorillonite (MMT), and NbO nanosheets (at concentrations of 1, 2, 5, 10 g L^{-1}), respectively, for the preparation of the nanocomposite-based hydrogels. All hybrid gels with nanosheets were prepared with 25 wt% F-127-DMA with respect to water. Then, 2 μL of 2-hydroxymethyl propiophenone as a photoradical polymerization initiator was added to 2 mL of these hydrogels.[6] A vortex device was used to mix the hydrogels. After homogenizing it at 4 °C, hydrogels were extracted with a syringe and gelled at room temperature. Hydrogels were extruded, formed into an arbitrary shape, and irradiated with UV light (365 nm) to perform photopolymerization.

Analyses

Atomic force microscopy (AFM) images were obtained with a Digital Instrument Nanoscope III microscope with a tapping mode. X-ray diffraction (XRD) patterns were recorded with a Rigaku RINT-1000 diffractometer (Mn-filtered FeK$_\alpha$ radiation) operating at a voltage of 40 kV, and a current of 30 mA, with a scan speed of 2.00° min^{-1}, and a step width of 0.02°. Inductively coupled plasma (ICP) emission spectrometry experiments were performed using of a Varian VISTA MPX CCD Simultaneous ICP OES instrument. Proton nuclear magnetic resonance (NMR) was performed with a JEOL JNM-ECX500. A sample was dissolved in deuterated chloroform and measured. Scanning electron microscopy (SEM) images were acquired with a JEOL IT-100 LA. Transmission electron microscopy (TEM) images were obtained with JEOL JEM-1011 microscope operating at 100 kV. The sample was dropped onto a carbon grid and vacuum dried. Thermogravimetry was performed with a Thermo plus 8120/EVO2 equipment in the range 20–800 °C at a heating rate of 10.0 °C min^{-1} under an air flow.

Rheological measurements

Rheological experiments were performed with the use of a modular compact rheometer (Anton Paar: MCR 102) and the use of a parallel plate (diameter of 25 mm). To avoid errors due to evaporation of water from both the hydrogels and the nanocomposites, the samples were surrounded by polymer trapping water. The temperature sweep of the rheological behavior was investigated by a time cure test at 1 Hz with a heating ramp rate of 1 K min^{-1}.

Results and discussion

Characterization of F127-dimethacrylate (F127-DMA)

The mechanisms of cross-linking DMA onto F127 are well described elsewhere. Briefly, the functionalization of F127 occurs with the reaction of the OH-terminated PEO-PPO-PEO triblocks with methacryloyl chloride. The reactive macromonomers were cross-linked by free radical polymerization. The functionalization of the OH-terminated PEO-PPO-PEO triblock was successfully confirmed by ^{1}H NMR. Proton NMR spectrum of F-127-DMA (Fig. S1 in ESI†) indicates that the average block length of polypropylene oxide is 59 and that the degree of polymerization (DP) reaches a value of 104. From the proton NMR data and the knowledge of the integrated area of the whole proton peaks, the total molecular weight was estimated to be 11 524 g mol^{-1}. After a comparison of the bulk F127 with those functionalized with DMA (F127-DMA), the degrees of DMA functionalization (f_n) were estimated to be 55%, 67%, and 88% indicating that the termination of the PEO moieties were functionalized by DMA at f_n degrees (ESI† Fig. S1 and Table S1).

Characterization of the nanosheets and their dispersions

In this study, several nanosheets were prepared to obtain a sufficient set of materials with different hydrophilic/phobic behaviors (Fig. 1) to reveal their impacts on the gelation as well as the elastic properties of F127-based nanocomposites. Raw Kunipia-F clay mineral, which exhibits a hydrophilic nature, was properly exfoliated in water by stirring, producing a dispersion of nanosheets showing a lateral size of about 1 μm
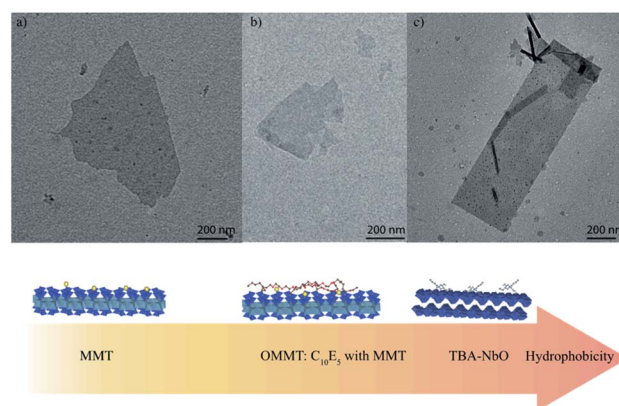

Fig. 1 Transmission Electron Microscopy (TEM) characterizations of the nanosheet dispersions of (a) raw hydrophilic montmorillonite (MMT); (b) organoclays (OMMT) prepared with montmorillonite as a starting material and the pentaethylene oxide monodecyl ether ($C_{10}E_5$) nonionic surfactants showing a hydrophobic–hydrophilic character; and (c) TBA-NbO exhibiting a hydrophobic behavior.

after the peeling procedure (Fig. 1a). Transmission electron microscopy (TEM) measurements revealed the absence of any aggregation (*i.e.* no dark areas attesting to an accumulation of matter were observed) and confirmed the proper exfoliation of the nanosheets which was also corroborated by atomic force microscopy measurements allowing us to obtain an accurate quantification of the thickness of the nanosheets which was about 1 nm.

Nonionic organoclay can be obtained through the intercalation of nonionic surfactants into the interlayer spaces of the raw clay mineral (Kunipia-F). The interaction mechanism leading to the adsorption of the poly(ethylene oxide) alkyl ethers (C_nE_m nonionic surfactants) involves ion–dipole interaction with the exchangeable sodium cations (*i.e.* the C_nE_m solvates the Na^+ ions just as water molecules do, Fig. S2 ESI†).[23,30] Due to the hydrophilic lipophilic balance value (HLB = 11.64) of the pentaethylene oxide monodecyl ether ($C_{10}E_5$) the resulting hybrid materials display a hydrophobic behavior with the arrangement of the amphiphile molecules in a monolayer organization, as could be confirmed by X-ray diffraction (not shown).[21,23,30] The dispersions of the organoclays (OMMT) were prepared in a similarly way to those of MMT leading to OMMT nanosheets with equivalent lateral size of about 1 μm (Fig. 1b).

The preparation of KNbO is well documented in the literature, and its characterizations by SEM, XRD, ICP and thermogravimetry (TG) analyses (ESI† Table S2 and Fig. S3–S6) allowed us to confirm the proper layered structure of the inorganic material and its chemical composition: $K_{3.72}Nb_6O_{17} \cdot 3.4H_2O$. The acidic treatment contributes to the release of potassium cations located within the interlayer I (the most reactive interlayer) of the hexaniobate layered materials that are exchanged with H^+. The latter H^+ are then cation-exchanged one more time with TBA, leading to the exfoliation of the TBA-NbO nanosheets. TEM observations showed very thin nanosheets with light contrast were observed (Fig. 1), suggesting the proper exfoliation of NbO. These nanosheets exhibited a lateral size of 1 μm and a thickness close to 1.90 nm, thus corroborating the proper exfoliation of NbO (expected value of 1.88 nm).[20]

All the nanosheet dispersions displayed a clear Tyndall effect due to the scattering of the colloids (here, nanosheets), suggesting that their proper dispersibility, which could stand for several months without any observable phase separations due to gravity or other mechanisms (ESI† Fig. S7).

Rheological properties of bulk F127-DMA hydrogels

The gelation of F127 Pluronic triblock copolymer with a nominal composition of $(EO)_{99}(PO)_{65}(EO)_{99}$ occurs with either an increase of the volume fraction of the F127 micelles or the temperature. Several mechanisms were suggested for the gelation formation. The close packing in a cubic array of the spherical micelles formed by F127 as well as the possible entanglements of the PEO hydrophilic groups contribute to the sol–gel transition. The latter transition could be also explained by a change in the entropy due to an arrangement of the water molecules in close interaction with the PO hydrophobic groups.[31,32]

We confirmed the importance of the concentration of F127 through both visual observations and rheological measurements in the gelation, where the temperature for the gelation formation, emphasized by a sharp increase in storage modulus, G' (Fig. S2 and S8 ESI†) as well as a cross-over between G' and G'', spread over 10 °C (15–25 °C) for the concentration range: 30–20 wt% of F127 respectively. Below 20 wt%, we could observe no gelation of F127 while F127–H_2O mixtures at concentration above 35 wt% display a high viscosity preventing the sol–gel transition to occur (ESI† Table S3). Since, the entanglements of hydrophilic PEO chains, especially if their molecular weights were larger than 1600 (case of F127), were suggested to be one of the key parameters in the gelation of the micelles, we first investigated first the impact of the terminal functionalization of the PEO chains by the dimethacrylate (DMA). The sweep temperature of the rheological characterization of F127 with different DMA functionalization rates of the PEO chains (f_n = 55, 67 and 88%) reveal closely similar evolution: with (i) a region where both G' and G'' show small values with the predominance of the viscous part in the complex shear modulus; (ii) abrupt increases in both G' and G'' and the crossover between G' and G'' in the contribution of the complex shear modulus; and (iii) a regime displaying slight continuous gradual growth reaching a plateau for G' and G'' with large values defining a hard gel state according to several studies (Fig. 2).

Interestingly, the terminal functionalization of the PEO chains with DMA does not affect the temperature for gelation which occurs at almost the same value of 18 °C, a result consistent with previous studies.[31–33] The entanglements of the PEO chains appears to play a minor role in the gelation of F127. Thus, the close packing of the micelles and their organization in clusters induced by hydrophobic interaction of the core PPO block seem to contribute principally to the gelation of F127. In addition to changing the volume fraction of the micelles locally and thus allowing their close packing or cluster formation, the increase in the temperature affects the dehydration of the PEO
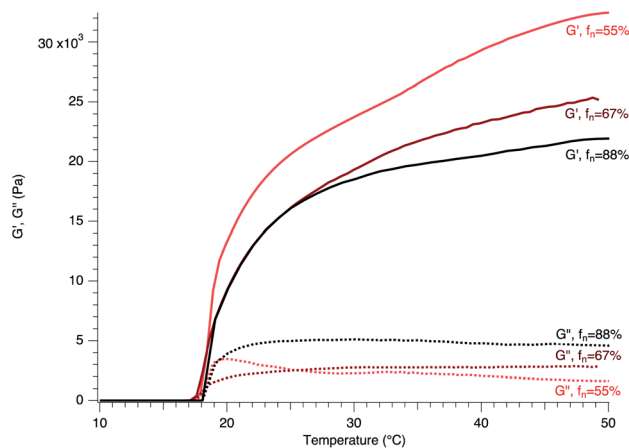
Fig. 2 Changes in both the storage (G', solid line) and loss (G'', dashed line) moduli as a function of temperature for Pluronic F127–H_2O at a concentration of 25 wt% with PEO chains functionalized by dimethacrylate (DMA) at different rates of 55, 67 and 88% highlighted in red, brown and black colors.

chains, whose hydrophilic nature gradually switches to hydrophobic leading to their possible mixing with PPO blocks and connection to other micelles for the gelation.[31–33]

If the terminal functionalization of the PEO chains by DMA does not affect the threshold value for the gelation by showing the same gelation temperature, the presence of DMA changes the elastic properties of the hydrogels with a decrease in the values of the storage modulus as f_n increases (Fig. 2). The termination of the PEO chains by DMA drives to a reduction of the storage modulus by a factor of 32% when f_n increases from 55 to 88% with almost the same factor. Although it appears tempting to relate the linear loss of the elastic properties of the thermo-responsive gels to the functionalization rate of the hydrophilic PEO blocks, additional samples with different DMA functionalization rates (and probably other moieties, *e.g.* methacrylate) need to be prepared to clearly emphasize the linear trend of the loss of the elastic properties with f_n. Nevertheless, the hydrogels with low f_n here display large G' values, underscoring the importance of the possible connection and interaction of the PEO chains between F127 that strengthen the elastic modulus of the hydrogels without affecting the threshold number of connections between the micelles for the gel formation.

Hydrogel based nanocomposites

In polymer-based nanocomposites, the inclusion of nanoparticles aims at reinforcing the global elastic properties of the resulting hydrogels or polymers as well as their hardness with the inclusion of crystalline materials (assuming their proper dispersion).[3,7,19] In addition, the inorganic particles may reinforce the cohesion of the hydrogels by forming potential physical and even chemical bonds with the F127 polymer or by generating a double network as might be illustrated by graphene oxide (GO) nanosheets, for instance, in sodium alginate hydrogel.[18] In this previous study, both GO morphology and geometry were assumed to be planar. However, when working with nanosheets which are somehow less flexible, fragile and soft systems than organic based colloids, it is rather common to observe other morphologies than that of the only expected planar one as Nakato *et al.*, emphasized with rolling up structures (30%) crumpled, fold and planar organizations that represent only 35% of the whole believed 'nanosheets' morphology. Similar organizations are also assumed with the use of the studied nanosheets. The hydrogel-based composites including nanosheets still display a Tyndall effect underscoring the proper dispersion of the whole nanosheets in the hydrogels with no phase separation observed. Their inclusion in the hydrogels including a large water content should not *a priori* dramatically modify their morphologies, and thus folded, crumpled, rolled and planar organizations are assumed to be found in similar proportions as those of the bulk systems. Since F127 includes two types of hydrophilic (PEO) and hydrophobic (PO) blocks, different nanosheets showing a hydrophilic, hydrophobic, and a dual hydrophilic–hydrophobic character for MMT, NbO and OMMT respectively were associated and their

impacts on both the gel formation and the elastic properties of F127 were investigated.

Clay minerals such as smectites are layered materials that show cation exchange capacities, and outstanding hydration properties.[21] These inorganic materials were previously and still are used for diverse environmental applications such as confinement matrices for radioactive wastes, passive geotechnical barriers in waste landfills, and adsorbents for the removal of both inorganic and organic pollutants in water remediation strategies.[21] Within the internal structure of smectites, water molecules are confined on various several scales: on a microscopic scale in the interlayer space of the layered materials with their intercalation in layers leading to the materials expansion at discrete values, in mesopores and on a macroscopic scale with the observation of the swelling of a material.

When dispersed in aqueous media, smectites such as raw Kunipia-F are delaminated or exfoliated with full access to the whole surface area of the inorganic material that can reach 750 $m^2 \ g^{-1}$. The resulting dispersions show a thixotropic behavior and act as a buffer for control of the pH. The dispersions of the phyllosilicate nanosheets result from attractive forces and repulsive electrostatic interaction between the negatively charged inorganic colloids screened by counterions (*e.g.* compensating cations) that can be explained by the Debye–Huckel theory. The excess of counterions in close interaction with the phyllosilicate nanosheet surface (Stern layer) implies a surplus of osmotic pressure contributing to a repulsive effect and ensuring in this way a proper dispersion of the nanosheets (Fig. S9 ESI†).

The association of these triblock copolymers to these colloidal dispersionseven at very low concentrations lies counter to the electrostatic effects as well as to the interfacial energy resulting from the presence of the nanosheets. The latter can easily affect the arrangement of the micelles facilizing or preventing their close packing as well as the entanglements and thus impacting the gelation and the elastic properties. Here, the addition of MMT dispersions at concentrations of 1 and 2 g L^{-1} to F127-DMA shifts the gelation to high temperatures with a reduction of the elastic properties of the hydrogel-based nanocomposites (Fig. 3). These observations underline the poor cohesion or affinity between the phyllosilicate sheets and F127. Despite the successful use of clay minerals for the adsorption of diverse organic molecules in a batch experiment context, raw clay minerals show some limits to hydrophobic nonionic compounds.[21] F127 micelles display a hydrophobic group with a hydrophilic PEO corona (which, however is functionalized with DMA but similar observations were obtained with other f_n), and a possible interaction between the raw clay colloids and F127 was expected. Nevertheless, in clay mineral dispersions, electrostatic effects may sensitively perturb the proper assembly of F127 micelles. Besides, the phyllosilicate nanosheets associating counterions are fully solvated through relatively strong ion–dipole interactions with water molecules. The latter screen the possible interaction with Pluronic F127 which thus show a poor affinity to the inorganic surface of the clay mineral. Similar observations were obtained with graphene oxide (GO) sheets where the hydrophobic PPO groups of F127

mainly interacted with the graphene patches of GO instead of the hydrophilic PEO groups.[34,35] Thus, in addition to inducing steric constraints, the interactions between water and MMT nanosheets require a larger energy for the proper diffusion of the micelles and their close packing. This led to an increase in the gelation temperature due to the lack of cohesion between the micelles for the two samples studied at different MMT concentrations showing almost the same behavior with the inclusion of crystalline particles as well as displaying a reduction in elastic properties in comparison to bulk F127-DMA.

The chemical modification of clay minerals represents a simple procedure with the use of both cationic or/and nonionic surfactants.[21] For the former, the modification and grafting of the amphiphilic molecules is achieved through a cation exchange, expelling the compensating inorganic cations. Depending on the density of the surfactant, different arrangements within the interlayer space can be observed: from a lateral to normal bilayer organizations that determine the final properties of the resulting organoclays. Nonionic surfactants are intercalated through ion–dipole interaction solvating the compensating cations.[23]

Whatever the type of surfactant used, the resulting composite materials or organoclays display a hydrophobic environment and an expansion of the interlayer space, promising properties for the use of organoclays as adsorbents for the removal of hydrophobic organic pollutants or as reinforcers to polymers for the preparation of polymer-based nanocomposites. In contrast to cationic surfactants showing antibacterial properties, organoclays prepared with nonionic analogous display an eco-environmentally friendly character and thus were successfully used as reinforcers to biodegradable polymers or as host matrices for the preservation of amino acids.[19,21]

The chemical modification of clay minerals with the use of surfactants screens out the repulsive forces and electrostatic effects without any aggregation of the particles (the grafting of the nanosheets by long alkyl chain surfactants contributes to steric repulsions preventing aggregation, as the observation of a Tyndall effect confirms, see Fig. S10 ESI†). Moreover, the nature of the pentaethylene oxide monodecyl ether ($C_{10}E_5$) nonionic surfactant appears equivalent to that of F127 with possible interaction of both species and enhancement of the entanglements between the micelles and the treated phyllosilicate sheets.

The results of the association of OMMT with F127-DMA show an enhancement of the elastic properties of the hydrogel-based nanocomposites with an increase up to 140% (Fig. 4). Furthermore, the incrementation of OMMT in F127 of which the proper dispersion was confirmed by the observation of a Tyndall effect (Fig. S10 ESI†) improves the elastic properties as well as shifts the gelation to lower temperature. The coverage of the phyllosilicate sheets by $C_{10}E_5$ facilitates the possible connections and interactions with F127 ensuring a proper cohesion within the nanocomposites. Thus, the hydrophobic character of the nanosheets appears as a linking or a cement, leading to a depression of the gelation temperature while enhancing the elastic behavior of the resulting materials.

The hexaniobate (NbO) nanosheets were treated with tetrabutylammonium, a short alkyl chain cationic surfactant allowing the whole coverage of the inorganic surface, and thus to obtain double layered nanosheets with a bold hydrophobic character (the interlayer II is rather unreactive preventing the full exfoliation of the hexaniobate). Dispersed in water, NbO nanosheets can form lyotropic liquid crystalline phases such as the lamellar phase for instance showing birefringence properties at very low concentrations. The formation of the liquid crystalline (LC) phases can be explained by the Onsager theory and are entropically driven. In a LC state, the organized nanosheets have a more accessible volume to explore locally thus maximizing the entropy as compared to a randomly isotropic state for the same volume fraction of the anisotropic colloids.[24]

These LC phases formed by NbO were already successfully associated with hydrogels conferring to the nanocomposites birefringence properties by maintaining the organization of the nanosheets.[7] Here, the hydrophobic nature of the NbO nanosheets as well as their stiffness considerably enhanced the elastic properties of the nanocomposites while showing a large depression of the gelation temperature (Fig. 5). Indeed, the storage modulus was increased by a factor of 160% while the gelation of the nanocomposites shifted to lower temperature by 4 °C. As previously explained, the gelation starts with dehydration of the hydrophobic blocks. As the temperature rises, the hydrophobic blocks are dehydrated allowing their aggregation or connection with other F127-DMA hydrophobic blocks. The presence of hydrophobic nanosheets may facilitate and contribute to the cohesion between the micelles. Thus, the inclusion of NbO nanosheets lowers the critical solution temperature for the entanglement or connection between the micelles leading to a gelation that occurs at a temperature of 14 °C.[12,23,24]

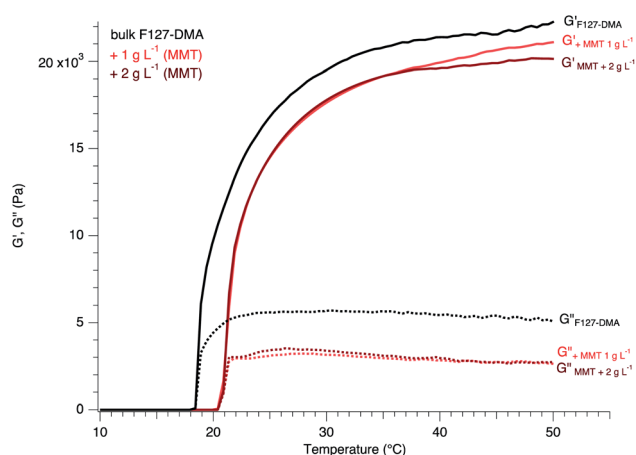Both Fig. 6 and 7 recapitulate and synthesize the precedent results allowing one to get a clear visualization of the
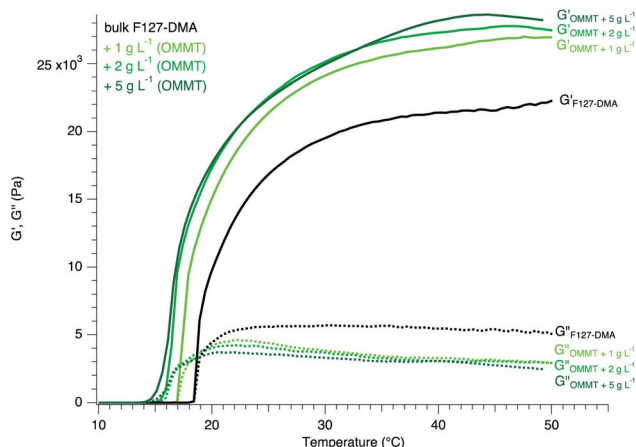

Fig. 3 Changes in both the storage (G', solid line) and loss (G'', dashed line) moduli as a function of temperature for Pluronic F127–H_2O at a concentration of 25 wt% with PEO chains functionalized by dimethacrylate (DMA) at a rate of 88% (black) and reinforced by or including dispersions of MMT at concentrations of 1 g L^{-1} (red) and 2 g L^{-1} (dark red).

Fig. 4 Changes in both the storage (G', solid line) and loss (G'', dashed line) moduli as a function of temperature for Pluronic F127–H$_2$O at a concentration of 25 wt% with PEO chains functionalized by dimethacrylate (DMA) at rate of 88% (black) and reinforced by or including dispersions of an organoclay (OMMT) at concentrations of 1 g L^{-1} (light green), 2 g L^{-1} (green) and 5 g L^{-1} (dark green).

differences between the whole samples and to stress out the importance of the nature of the nanosheets. As previously explained, the colloidal dispersions are characterized by an important interfacial energy and the systems are stabilized by a delicate balance of attractive and repulsive forces between nanosheets and the F127 micelles. In addition, the inclusion of the nanosheets represents a certain volume that is not more accessible (excluded volume) to F127, leading to possible frustration, exclusion or cohesion between the colloids depending on their chemical affinity.

For hydrophilic MMT nanosheets, the sol–gel transition occurs at a temperature higher than that of bulk F127-DMA hydrogel due to the retention of water by the phyllosilicate

sheets. The solvation of the MMT nanosheets prevents further interaction with F127 micelles and especially the PEO chains at low temperature and their presence significantly affect the hydrophobic network formed by F127 micelles. As a result, the gelation temperature is shifted to high temperature while the storage modulus is reduced as compared to that of bulk F127-DMA.

In contrast, when hydrophobic nanosheets such as OMMT are associated, the gelation appears to be favored and temperature depressed. In addition, the hydrogel nanocomposites including OMMT display a larger G' than bulk hydrogels. At an OMMT concentration of 5 g L^{-1}, the increase in G' is 31% larger than that of bulk F127-DMA hydrogel, and is maximal. As previously discussed, the presence of the hydrophobic nanosheets enhances the connections between the colloidal objects improving the global elastic properties of the nanocomposites. In hydrogel systems, several studies have pointed out the importance of the contribution of hydrophobic materials to the improvement of the mechanical behavior with an increase in the storage modulus.[36] Here, the inclusion of hydrophobic nanosheets follows the same trend. Similarly, due to the grafting of TBA onto the NbO nanosheet surface, the cross-linking between F127 and the NbO nanosheets might be enhanced and the gelation occurs at low temperature with a shift of about 4 °C in contrast to the bulk F127-DMA. The entanglements between F127-DMA micelles and NbO nanosheets due to hydrophobic interaction leads to "robust" hydrogels with a storage modulus G' 48% larger than that of the bulk system.

Finally, the introduction of hydrophobic nanosheets into the hydrogel network not only improves the mechanical properties of the nanocomposite, but it also enables tuning of the gelation formation that is shifted to low temperature. The process shows promise for further applications with the use of polymers at low concentrations or for systems in which no sol–gel transition can be observed. Last but not the least, while showing a large water
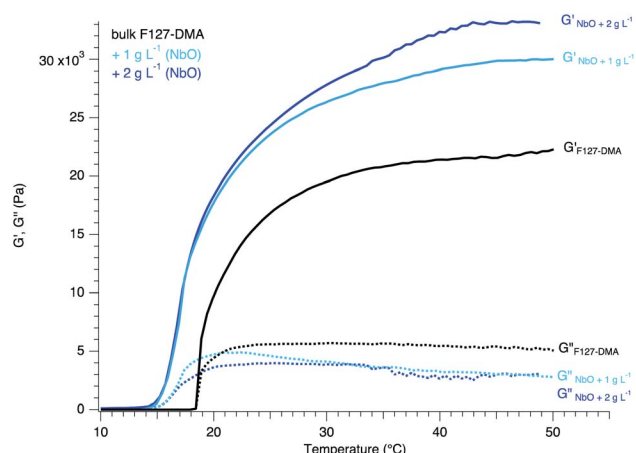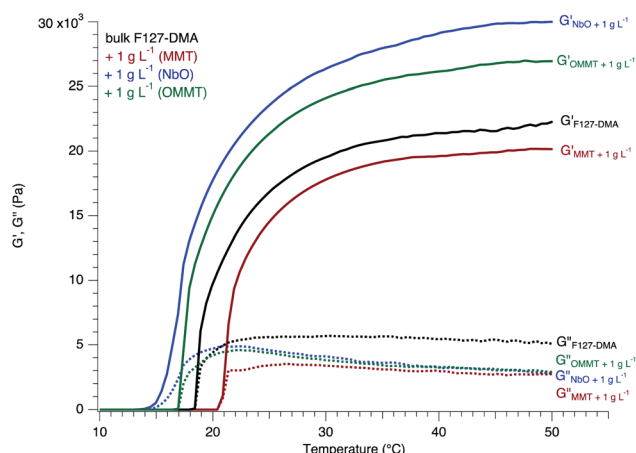

Fig. 5 Changes in both the storage (G', solid line) and loss (G'', dashed line) moduli as a function of temperature for Pluronic F127–H$_2$O at a concentration of 25 wt% with PEO chains functionalized by dimethyl acrylate (DMA) at a rate of 88% (black) and reinforced by or including a dispersion of TBA-NbO at concentrations of 1 g L^{-1} (light blue) and 2 g L^{-1} (dark blue).

Fig. 6 Changes in both the storage (G', solid line) and loss (G'', dashed line) moduli as a function of temperature for Pluronic F127–H$_2$O at a concentration of 25 wt% with PEO chains functionalized by dimethyl acrylate (DMA) at a rate of 88% (black) and reinforced by dispersions of MMT (dark red), NbO (blue) and OMMT (green) at a concentration of 1 g L^{-1}.
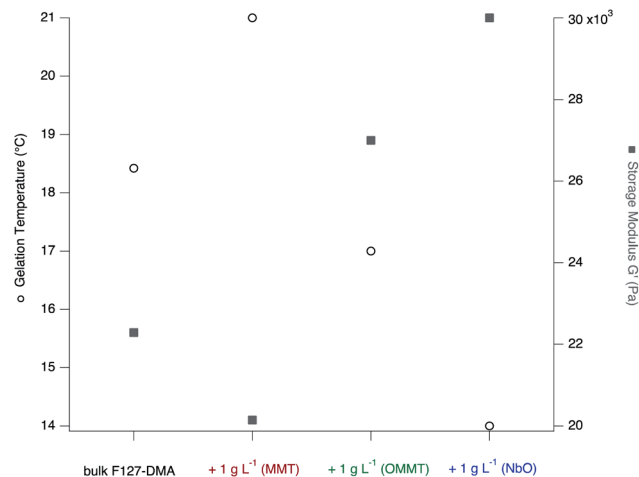
Fig. 7 Evolution of the gelation temperature and the storage modulus of bulk F127-DMA hydrogel and the hydrogel based nanocomposites prepared with MMT, OMMT and NbO at a concentration of 1 g L^{-1}.
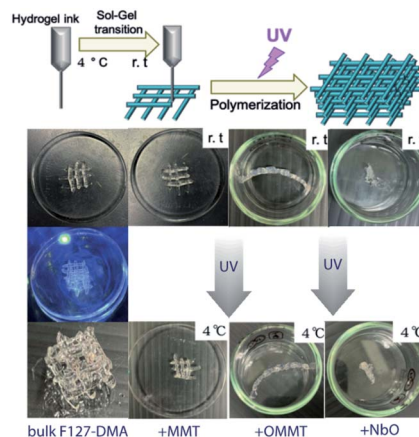

Fig. 8 Schematic representation and appearances of the 3D structures created after photopolymerization by UV radiation using F127-DMA in water at a concentration of 25 wt% and the hydrogel nanocomposites reinforced with MMT, OMMT and NbO.

content (estimated at up to 50 wt% by thermal gravimetry analyses – not shown), the whole hydrogel-based nanocomposites can be photo-polymerized through UV radiation and thus can be used as potential matrices for the confinement and preservation of bio-organisms[9] (Fig. 8). While the temperature affects the morphologies of the micelles and favors the flexibilities and dynamics of the PEO chains functionalized by DMA and their possible entanglements as well as impacting the water content and the volume fraction of F127, the composites are principally polymerized by light exposure. The polymerization through UV radiation was performed when all the samples underwent the gelation occuring at low temperature for the whole studied hydrogels as well as their derivative composites and the resulting materials showed solid and robust structures (Fig. 8). At low temperature when the samples are in sol state, the polymerization was still possible suggesting that the main mechanism in cross-linking the hydrogels bears leans more toward on a photophysical process than toward a thermal one, while the temperature draws on the characteristics and properties of the hydrogels as explained previously.

Conclusions

Thermo-responsive hydrogels have received considerable attention due to their singular mechanical properties and have been used as potential drug delivery systems or biocompatible matrices for different bio-organisms such as yeasts. In this study, the terminals of Pluronic F-127 triblock nonionic copolymer were functionalized by dimethacrylate (DMA) moiety at different rates f_n and its impact on the gelation as well as the elastic properties was investigated. The resulting F127-DMA show similar thermo-reversible sol–gel transition temperature for all f_n, while the elastic properties narrowly linked to the entanglements or connections between the micelles are reduced with the functionalization of the PEO chains by DMA.

The chemical nature of nanosheets (hydrophobic or hydrophilic) has significant consequences for gelation with an increase in temperature for hydrophilic MMT and a reduction in temperature for hydrophobic colloids. In the latter case, the affinity of the core of the F127 micelles for the hydrophobic surface of the nanosheets facilitates the cohesion and entanglements, ensuring production of elastic materials whose storage modulus is larger than that of bulk F127-DMA at the same concentration in water. The resulting materials are still defined as soft gels (while their classification mainly depends on their concentration and usage temperature range) but show some notable differences at high temperature and low water content where the storage modulus value increases up to 25% after the inclusion of the hydrophobic double nanosheets (hexaniobate) while the entanglements in hydrogels including hydrophilic MMT nanosheets decrease. The inclusion of the nanosheets impacts the elastic properties by showing large variations in the storage modulus while the loss modulus with its remaining high water content shows fewer variations in its value. All the prepared hydrogel-based nanocomposites enable control of the gelation temperature that can be depressed to very low temperature, something that could be not be achieved using only bulk Pluronic triblock copolymers.

Conflicts of interest

There are no conflicts to declare.

Acknowledgements

Notes and references

1 S.-k. Ahn, R. M. Kasi, S.-C. Kim, N. Sharma and Y. Zhou, *Soft Matter*, 2008, **4**, 1151–1157.

2 L. C. Gerber, F. M. Koehler, R. N. Grass and W. J. Stark, *Proc. Natl. Acad. Sci.*, 2012, **109**, 90.

3 Y. Kamachi, B. P. Bastakoti, S. M. Alshehri, N. Miyamoto, T. Nakato and Y. Yamauchi, *Mater. Lett.*, 2016, **168**, 176–179.

4 L. Klouda and A. G. Mikos, *Eur. J. Pharm. Biopharm.*, 2008, **68**, 34–45.

5 L. Li and Y. Aoki, *Macromolecules*, 1997, **30**, 7835–7841.

6 X. Liu, T.-C. Tang, E. Tham, H. Yuk, S. Lin, T. K. Lu and X. Zhao, *Proc. Natl. Acad. Sci.*, 2017, **114**, 2200.

7 N. Miyamoto, M. Shintate, S. Ikeda, Y. Hoshida, Y. Yamauchi, R. Motokawa and M. Annaka, *Chem. Commun.*, 2013, **49**, 1082–1084.

8 C. A. Mora, A. F. Herzog, R. A. Raso and W. J. Stark, *Biomaterials*, 2015, **61**, 1–9.

9 A. Saha, T. G. Johnston, R. T. Shafranek, C. J. Goodman, J. G. Zalatan, D. W. Storti, M. A. Ganter and A. Nelson, *ACS Appl. Mater. Interfaces*, 2018, **10**, 13373–13380.

10 A. Vedadghavami, F. Minooei, M. H. Mohammadi, S. Khetani, A. Rezaei Kolahchi, S. Mashayekhan and A. Sanati-Nezhad, *Acta Biomater.*, 2017, **62**, 42–63.

11 A. B. Dababneh and I. T. Ozbolat, *J. Manuf. Sci. Eng.*, 2014, **136**(6), 061016.

12 G. Dumortier, J. L. Grossiord, F. Agnely and J. C. Chaumeil, *Pharm. Res.*, 2006, **23**, 2709–2728.

13 S. V. Murphy and A. Atala, *Nat. Biotechnol.*, 2014, **32**, 773–785.

14 A. Lode, F. Krujatz, S. Brüggemeier, M. Quade, K. Schütz, S. Knaack, J. Weber, T. Bley and M. Gelinsky, *Eng. Life Sci.*, 2015, **15**, 177–183.

15 S. Wüst, M. E. Godla, R. Müller and S. Hofmann, *Acta Biomater.*, 2014, **10**, 630–640.

16 N. Gjerde, K. Zhu, K. D. Knudsen and B. Nyström, *Eur. Polym. J.*, 2019, **112**, 493–503.

17 M. Müller, J. Becher, M. Schnabelrauch and M. Zenobi-Wong, *Biofabrication*, 2015, **7**, 035006.

18 J. Fan, Z. Shi, M. Lian, H. Li and J. Yin, *J. Mater. Chem. A*, 2013, **1**, 7433–7443.

19 L. N. Carli, T. S. Daitx, R. Guégan, M. Giovanela, J. S. Crespo and R. S. Mauler, *Polym. Int.*, 2015, **64**, 235–241.

20 Y. Chen, K. Zheng, L. Niu, Y. Zhang, Y. Liu, C. Wang and F. Chu, *Int. J. Biol. Macromol.*, 2019, **128**, 414–420.

21 R. Guégan, *C. R. Chim.*, 2019, **22**, 132–141.

22 S. Li, Z. Yang, J. Xu, J. Xie and J. Sun, *J. Compos. Mater.*, 2019, **53**, 315–326.

23 R. Guégan, E. Veron, L. Le Forestier, M. Ogawa and S. Cadars, *Langmuir*, 2017, **33**, 9759–9771.

24 R. Guégan, K. Sueyoshi, S. Anraku, S. Yamamoto and N. Miyamoto, *Chem. Commun.*, 2016, **52**, 1594–1597.

25 H. Ding, S. T. Khan, J. Liu and L. Sun, *Gels*, 2021, **7**, 106.

26 E. W. Hansen, P. Norby, J. Roots and Q. Wu, *J. Phys. Chem. C*, 2007, **111**, 11854–11861.

27 D. Ma, J. Lin, Y. Chen, W. Xue and L.-M. Zhang, *Carbon*, 2012, **50**, 3001–3007.

28 R. R. Mehra, P. Tiwari, A. Basu and A. DuttKonar, *New J. Chem.*, 2019, **43**, 11666–11678.

29 R. Zhang, Q. Ding, S. Zhang, Q. Niu, J. Ye and L. Hu, *Nanoscale*, 2019, **11**, 12553–12562.

30 R. Guégan, *J. Colloid Interface Sci.*, 2011, **358**, 485–490.

31 K. Hyun, J. G. Nam, M. Wilhellm, K. H. Ahn and S. J. Lee, *Rheol. Acta*, 2006, **45**, 239–249.

32 M. J. Park and K. Char, *Macromol. Rapid Commun.*, 2002, **23**, 688–692.

33 M. Jalaal, G. Cottrell, N. Balmforth and B. Stoeber, *J. Rheol.*, 2016, **61**, 139–146.

34 Y. Yan, L. Piao, S.-H. Kim, W. Li and H. Zhou, *RSC Adv.*, 2015, **5**, 40199–40204.

35 S.-Z. Zu and B.-H. Han, *J. Phys. Chem. C*, 2009, **113**, 13651–13657.

36 D. Cohn, A. Sosnik and S. Garty, *Biomacromolecules*, 2005, **6**, 1168–1175.